# Effect of impressed current on the microstructure of corroded steel-concrete interface

**R. Ghanti**[1]

1. Imperial College London, Civil Engineering Department, UK

Correspondence to: Rudrabir Ghanti (rudrabir.ghanti@yahoo.com)

**Abstract**

The alkaline nature of concrete ensures that the corrosion initiation of reinforcing steel embedded in concrete takes a long time. Concomitantly, accelerated corrosion tests were carried out using impressed current till the crack initiation phase occurred as a result of which the testing period was reduced from years to a few weeks. An electrochemical cell was set up and direct current was impressed from the titanium mesh (acting as cathode) to the rebar (anode) through the concrete with the help of sodium chloride solution (electrolyte). Back-scattered electron images were obtained on flat, polished samples followed by image analysis to study the amount and distribution of corrosion products around the steel-concrete interface. It was found that impressed current technique was successful in simulating the natural corrosion process in terms of corrosion pattern, distribution and method of attack. The amount of steel loss did not increase in proportion to corrosion current as suggested by Faraday's law. Other micro-structural factors like extent of micro-cracking, dense accumulation of corrosion product at the steel-concrete interface may play a significant role in steel section loss especially at higher corrosion rates. The degree of corrosion of ribbed bars was found to be more as compared to plain bars. Moreover, ribbed bar samples had a greater uneven and heterogeneous corrosion product distribution than plain bars. A detailed characterisation of the effect of accelerated corrosion on the microstructure of the corroded steel-concrete interface is discussed.

## 1 Introduction and Objective

Chloride ions are known to be most mobile and it is one of the primary reasons for deterioration of reinforced concrete structures. The source of these chloride ions are primarily seawater and de-icing salts sprayed on highways and bridges for maintenance. The natural concrete medium is very basic mainly due to the pore solution of the cement paste which comprises of alkalis like sodium and potassium, keeping the pH around 13. However, the ingress of chloride ions through the pores of concrete may lower the pH, attack the steel surface and cause it to de-passivate. As the steel corrodes via electrochemical reaction, it is converted into rust products which have a volume two to six times higher than the steel consumed. After accommodating itself within the porous cement paste during the free expansion step (Wong et al., 2010; Liu &Weyers, 1998), the corrosion products are accumulated at the steel concrete interface where they exert expansive tensile stress on the walls of the surrounding cement paste. Once the stress exceeds the tensile strength of concrete the

concrete cover cracks; thereby resulting in de-lamination and spalling.

Numerous models (Andrade, Alonso & Molina, 1993; Wong et al., 2010) have been developed to predict the time needed for cracking of chloride contaminated structures (Liu &Weyers, 1998; Allan, 1995; Tuutti, 1982; Bazant, 1979). Among them, Tuutti's model is most widely accepted which advocates that corrosion occurs in two stages: initiation and propagation. The corrosion initiation stage is considered to be the most dominant phase in the corrosion process depending on the corrosion resistance of the reinforcement, thickness and quality of concrete cover, chloride threshold concentration, mix composition (Chen &Mahadevan, 2008). The diffusion of chloride ions into the cement paste may cause the dissolution of iron by forming chloro-complexes (Green Rust) which migrate within the pore structure and precipitate into higher volume corrosion products in the presence of oxygen causing damage (Sagoe-Crentsil&Glasser, 1993). Occasionally, lower expansive corrosion products are formed when the oxygen supply is low leading to the formation of "black rust" which does not provide any visual warning like above (Bentur, Diamond &Berke, 1997).

The natural corrosion process is usually slow and takes a long time to initiate. Hence, various accelerated tests have been developed to reduce the time taken to cause corrosion. Impressed current is one such technique where chloride diffusion is enhanced by setting up an electrochemical cell with reinforcing steel acting as anode and counter electrode like titanium mesh is made cathode. An electric current is applied with chloride solution as an electrolyte. This method allows reducing the testing period from years to a few weeks; thus saving money as well. It also offers a better control over the corrosion rate which is a function of changes in the resistivity, oxygen concentration and temperature. Although, this technique is beneficial in terms of applying a constant current but may artificially influence the formation and distribution of corrosion products. Past studies (Care &Raharinaivo, 2007; El Maaddawy&Soudki, 2003; Gonzalez et al., 1995; Andrade, Alonso & Molina, 1993) have indicated that the longitudinal surface crack formation parallel to rebar, corrosion product distribution and method of steel attack for impressed current reinforced mortar specimens resemble the natural condition very closely. The extent of steel section loss for a given corrosion current can be found from Faraday's law (Broomfield, 2007). It suggests that the steel attack penetration increases in proportion to the corrosion current applied. The type of rebar whether deformed or plain also has a significant impact on the degree of steel loss (Mohammed et al., 2001).

Various studies have looked into composition and distribution of corrosion products around the steel-concrete interface using alternate wetting and drying as the accelerated corrosion test (Wong et al., 2010; Jaffer& Hansson, 2009; Poupard et al., 2006; Jensen et al., 1999). However, very few have tried to characterise the effect of impressed current on the distribution of corrosion products around the steel bar.

Consequently, within the current context, the main aim of this study is to characterise the amount and distribution of corrosion products around the corroded steel-concrete interface for impressed current specimens and validate their results with the alternate wetting and drying sample. Attempts have also been made to study the rust growth and cracking patterns at the steel-concrete interface especially at higher corrosion currents and compare with the theoretical steel loss obtained from

Faraday's law. Finally, the corrosion extent and distribution for ribbed and plain bar specimens have also been compared.

## 2 Experimental Program

### 2.1 Materials

CEM 1 type Portland cement (EN 197-1:2000) was used (Table 1).

**Table1:** Phase composition of unhydrous cement with XRD-Rietveld

| **Phases** | **CEM 1 unknown: average wt%** |
|---|---|
| Alite ($C_3S$) | 64.5 |
| Belite ($C_2S$) | 16.2 |
| Ferrite ($C_4AF$) | 8.7 |
| Aluminate ($C_3A$) | 6.7 |

Crushed limestone and sharp sand having maximum size of 10 mm and 5 mm respectively, were used as aggregates. The test specimens comprised both ribbed and plain steel bar (Table 2). The source of chloride was a 3% NaCl solution. Potable tap water was used as mixing water.

**Table 2:** Chemical composition of rebar used.

| **Composition (%)** | **C** | **Mn** | **Si** | **S** | **P** |
|---|---|---|---|---|---|
| **Ribbed bar** | 0.19 | 0.55 | 0.19 | 0.02 | 0.02 |
| **Plain bar** | 0.11 | 0.50 | 0.157 | 0.015 | 0.015 |

### 2.2 Specimens

Corrosion induced cracking is a function of cover depth, diameter of rebar, water cement ratio (W/C), mix-proportion, cast position of the bar, corrosion rate, etc. Thus, in order to study the effect of accelerated corrosion tests on distribution of corrosion products around the steel-concrete interface, all the other variables were kept constant except corrosion rate. The mixture proportion for all the five specimens is summarized in Table 3.

**Table 3:** Mixture Proportions

| **Water/ Cement ratio** | **CEM 1 (kg/m$^3$)** | **Water (kg/m$^3$)** | **Limestone (kg/m$^3$)** | **Sand (kg/m$^3$)** |
|---|---|---|---|---|
| 0.5 | 350 | 175 | 1160 | 740 |

The layout of the specimen is shown in Fig. 4. One 10 mm steel bar was embedded horizontally in each of the five specimens at a cover depth of 10 mm. A lower cover depth ensured earlier corrosion initiation.

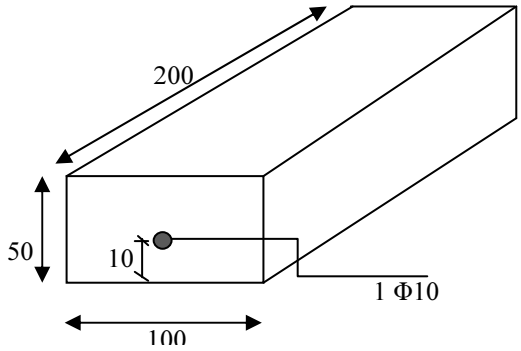


**Fig. 1**: Layout of the specimen.

The specimens were casted normally and cured for a period of 28 days at 100% relative humidity to avoid moisture loss and premature shrinkage cracking. The rebar was extended from the end of the specimen to allow polarization of the reinforcement anodically during the application of impressed current.

**Table 4:** Specimen guide along with current intensities

| **Speci-men No.** | **Type of rebar** | **Current intensity (µA/cm$^2$)** | **Sample labelling(after sectioning, polishing, grinding and carbon coating)** |
|---|---|---|---|
| 1 | Ribbed | 1 | 1R |
| 2 | Ribbed | 10 | 10R |
| 3 | Ribbed | 100 | 100R |
| 4 | Plain | 100 | 100P |
| 5 | Plain | Alternate wet/ dry | WDP |

### 2.3 Accelerated corrosion test program

The specimens 1, 2, 3, and 4 which were subjected to impressed current had an experimental set-up as shown in Fig. 2. The bottom face of the specimen was immersed in a 3% NaCl solution (30 g/L). This ensured that chloride penetration occurred primarily through the bottom cover. This approximated real size structural elements exposed to ground conditions or car parking areas where chloride transport is mainly unidirectional. The rebar was connected to the positive terminal of the power supply and thus behaved as anode. Whereas, the counter electrode, made of titanium mesh, was placed underneath the reinforced concrete specimen and connected to the negative terminal. A constant direct current was impressed on the steel reinforcing bar by means of power supply and a resistor was used to control the flow of current in the system.

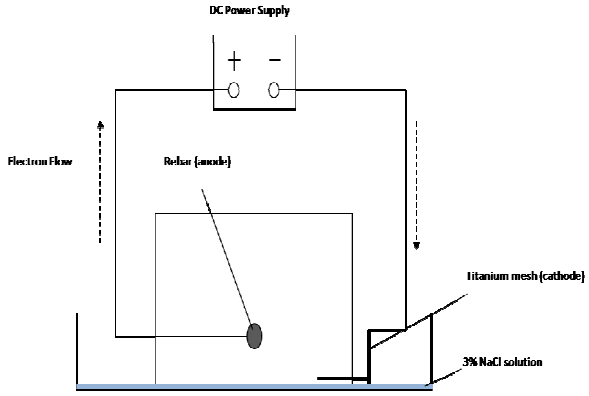


**Fig. 2**: Experimental set up for impressed current technique.

On the contrary, the bottom surface of specimen 5 was immersed in a 3% NaCl solution followed by drying at 20° C. Each wet/dry cycle lasted for 3.5 days. Consequently, this would enable comparison on the effect of two different accelerated corrosion techniques viz., impressed current and alternate wetting/drying on the microstructure of the corroded steel-concrete interface.

In both cases i.e. impressed current and alternate wetting/drying, corrosion tests were carried on till the first visible crack appeared (crack width below 0.015 mm), i.e. crack initiation stage. Magnification lens in conjunction with microscope were used to trace out the crack length and average crack width.

### 2.4 Sample preparation for BSE imaging

Once the initial cracks appeared, the specimens were oven dried at 40° C followed by epoxy treatment on the bottom surface. The specimens were carefully cut with a diamond saw into sections having a dimension 95 mm x 22 mm x 8 mm (Fig. 3). The sectioning was done at the middle of the cracks. The labelling used for these sectioned samples has been tabulated in Table 4. The sectioned samples were dried at 50° C and then embedded with epoxy resin (except the bottom face which is the area of interest) to protect the microstructure from damage. The bottom face was fine ground using dry silicon carbide papers of grit sizes 500, 1000 and 1200 followed by cleaning with acetone. The dried sample was then vacuum-impregnated with low viscosity epoxy resin to fill any cracks/pores which ensured better imaging. This was again succeeded by grinding as before and polishing with non woven cloths fixed with diamond abrasives of sizes 9, 6, 3, 1 and 1/4 μm. The polishing time was kept short to minimize the surface relief. Despite all the precautions taken to produce a well polished sample, a few fine cracks resulted in the interface. Possible reasons could be drying shrinkage of the cement paste, differential expansion during oven drying and cutting/polishing materials of different hardness. The high vacuum SEM conditions meant that conductive carbon coating of the flat-polished sample was required to avoid the build up of excessive negative charge which may hamper the signal and contrast quality of the sample (Goldstein et al., 2003).

**Fig. 3**: Image of a flat-well polished carbon coated sample to be used for SEM imaging.

### 2.5 BSE imaging and EDX microanalysis

The corroded steel-concrete interface was examined using scanning electron microscope. BSE images were obtained on the polished samples to study the distribution of corrosion products at the interface. The intensity of the BSE increases with the atomic number of the phase and provides a good measure for segmenting the various phases within a microstructure. The grey scale of the phases arranged in terms of brightness levels are steel (lightest) > anhydrous cement particles > calcium hydroxide (CH) > calcium silicate hydrate gels ~ calcium-aluminate hydrates ~ aggregates > porosity and voids which appears as the darkest phase (Zhao & Darwin, 1992).

In order to conduct elemental analysis and chemical characterization of the corrosion layer phase of 1R, 10R and 100R, an EDX microanalysis was carried out.

### 2.6 Image analysis

The stitched image was then imported into Image J (Rasband, 1997), an image processing program developed at the National Institute of Health (USA).

This program was used to calculate the un-corroded steel area, amount of corrosion layer (abbreviated as CL- this is the layer of corrosion products which accumulates at the steel-concrete interface), corrosion paste (abbreviated as CP- affected cement paste containing high Fe penetration), fraction of perimeter affected and extent of micro-cracks after calibrating the scale of the images suitably. Two methods for estimating CL and CP area were considered, viz. point count analysis and manual segmentation with free hand selection tool based on differences in grey scale levels. However, it was decided to stick with the latter option.

## 3 Result

### 3.1 Visual Inspection

All the specimens were subjected to corrosion tests till the first visible crack (having a minimum crack width of 0.015 mm) appeared on the bottom surface. The surface cracks developed parallel and directly below the rebar as has been reported in previous studies (El Maaddawy&Soudki, 2003; Cabrera, 1996). The cracks were discontinuous and had variable crack widths (Table 5).

**Table 5:** Quantification of surface crack intensity along with time needed.

| Specimen (Label) | Crack length (mm) | Average crack width (μm) | Time to first visible crack (days) |
|---|---|---|---|
| 1 (1R) | 15.8 | 15.8 | 154 |
| 2 (10R) | 30 | 20.6 | 45 |
| 3 (100R) | 5.2 | 14 | 14 |
| 4 (100P) | 3.8 | 15.7 | 14 |
| 5 (WDP) | 35 | 28.9 | 292 |

Expectedly, the time to cracking decreases as we increase the corrosion current intensity. This can be attributed to the fact that a lower corrosion rate would lead to a lower steel section loss and cause a gradual dissipation of corrosion products in the pore structure of concrete leading to a gradual build up of radial pressure and hence, cracking (Mangat&Elgarf, 1999). However, specimen 5 took the longest time to crack as it simulated a real

situation (alternate wet/dry) where corrosion currents are generally very low.

The crack intensity patterns observed for impressed current specimens were found to be very interesting. The average crack width increased till 10 μA/cm$^2$ followed by a reduction for 100 μA/cm$^2$. To our knowledge, such a variation in crack width has not been reported before. In our case, both 10R and 100R had quite similar corrosion degree i.e. 0.8% (Table 6- column 2) but yet 10R had a slightly higher surface crack width. A possible explanation could be increased micro-cracking (Fig. 4) around the steel-concrete interface at higher current densities which help to relieve the internal stress leading to a reduced surface crack width in case of 100R. A similar pattern was also observed for surface crack length which could again be rationalized based on similar reasons.

Specimen 4 showed a marginally higher crack width than specimen 3 but had a smaller crack length. This is consistent with previous studies where plain bars showed fewer but wider corrosion induced cracks than ribbed bars (Mohammed et al., 2001).

The specimen 5 demonstrated the highest average crack width and length. This is due to gradual build up of corrosion products accumulated within the paste and steel-concrete interface over a longer period of time which produces a large expansive pressure leading to increased crack intensity.

The extent of corrosion damage was very small for all the specimens owing to the fact that corrosion tests were carried on till the crack initiation stage only. Moreover, the corrosion products were not homogeneously distributed along the bottom of the rebar (as can be seen later in Figs. 5-7). The colour of the corrosion product was primarily dark brownish- red with traces of green rust.

### 3.2 Extent of corrosion induced micro-cracking

Due to the accelerated nature of corrosion tests, the extent of corrosion- related damage (in terms of area fraction of cracks) was very small. Corrosion induced micro-cracks tend to progress from the corrosion layer towards the concrete cover. It was noted that these micro-cracks preferentially advanced along the aggregate rather than bulk cement paste. A possible reason could be the structural inferiority of ITZ (Interfacial Transition Zone) along the aggregate-matrix interface which promotes the propagation of cracks along them.

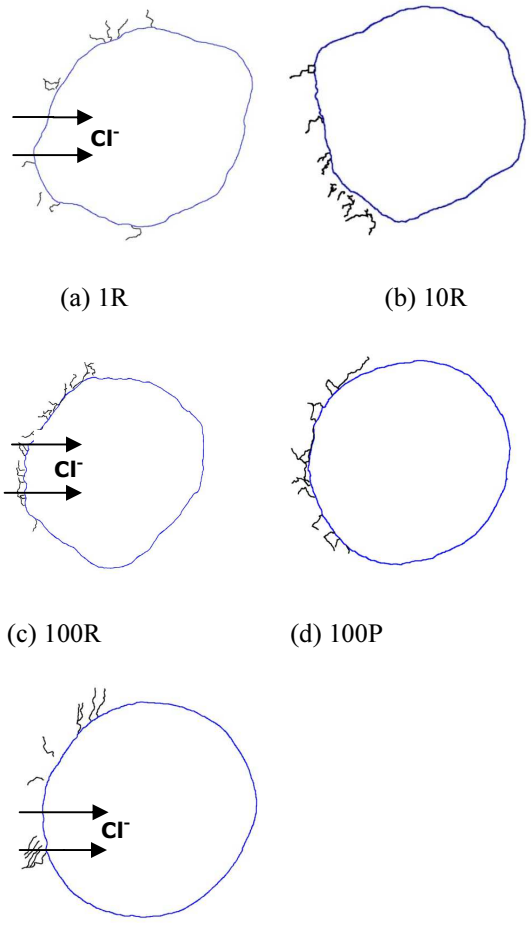


(a) 1R (b) 10R

(c) 100R (d) 100P

(e) WDP

**Fig.4**: Distribution of micro-cracks around the rebar at a distance of 700-800 μm from steel. (Corrosion source was on left side)

Fig. 4 shows distribution of micro-cracks around steel interface. It is clearly visible that the extent of micro-cracking is more in the case of 100R sample. The greater number of micro-cracks i.e. relieves the rapidly built up stress concentration and vindicates our previous observation (Table 5) that 100R sample had a smaller average surface crack width.

### 3.3 Quantitative estimation of corrosion products at the steel-concrete interface

Table 6 represents the steel section loss computed experimentally and compared to the steel loss obtained from Faraday's law (Broomfield, 2007):

$$M = 11.6 \times I \times t$$

where M= steel section loss (μm), I= corrosion current intensity (μA/cm$^2$), t= time in years since the current was applied, and 11.6 = conversion factor from μA/cm$^2$ to μm/year assuming homogeneous corrosion. Thus, for 1R sample the amount of section loss as per Faraday's law would be: M= 11.6*1*154/365 = 4.89 μm.

**Table 6:** Steel section loss obtained from experiment v Faraday's law.

| Sample | Degree of corrosion (%) | Steel section loss from experiment (μm) | Steel section loss from Faraday's law (μm) |
|---|---|---|---|
| 1R | **0.56** | **23.41** | 4.85 |
| 10R | **0.76** | **55.84** | 14.17 |
| 100R | **0.81** | **49.54** | 44.109 |
| 100P | **0.64** | **41.25** | 44.109 |
| WDP | **1.07** | **81.34** | - |

Experimentally, 10R showed slightly higher steel section loss than 100R. Ideally, degree of corrosion and steel section loss should follow a similar pattern with increase in corrosion current but the variation could be attributed to the different original rebar areas which in turn, depend on the section from where the steel was taken. Owing to this fact, degree of corrosion (measured in %) would provide a better alternative to interpret the corrosion damage rather than steel section loss (measured in absolute terms). Nonetheless, considering Faraday's law, one would still expect that the steel section loss should increase significantly with an increase in impressed current but this is clearly not the case with 10R and 100R samples which have comparable levels of steel loss (49-55 μm). A possible explanation for such a trend has been discussed below:

Reasons for comparable steel section loss for 10R and 100R: An increase in corrosion rate leads to an increased corrosion induced micro-cracking (Fig. 4). These micro-cracks have an impact on the transport properties on concrete (Wong et al., 2009) and enhance the chloride and oxygen diffusion along with water sorpvity. Thus, the increased supply of oxygen and moisture (in the case of 100R sample) results in the formation of higher volume corrosion products which produces a high expansive stress at the steel-concrete interface. The higher oxidation level in the corrosion layer for 100R sample has been confirmed by EDX analysis. This expansive stress at the steel-concrete interface eventually leading to cover cracking can be produced by two ways:

- A large accumulation of small volume corrosion products which would mean a larger steel section loss (as seen in the case of 10R sample).
- A relatively smaller accumulation of larger volume corrosion products (caused by higher oxidation) which points to a smaller steel section loss (as manifested by 100R sample).

Moreover, a denser formation of corrosion products at the steel-concrete interface can affect the mobility of $Fe^{2+}$ and $OH^-$ ions across the corrosion layer which poses a question on the ability of Faraday's law to predict steel losses at higher corrosion rates(El Maaddawy&Soudki, 2003). Thus, the above reasoning justifies the observation that at higher impressed current i.e. 100 $\mu A/cm^2$ we may not get proportionally higher steel loss as suggested by Faraday's law.

The extent of corrosion and steel loss for 100R sample was more than 100P sample.

The WDP sample showed the highest degree of corrosion and rebar loss. This was expected as WDP sample took the longest time to crack indicating a gradual build up of corrosion products. The corrosion products formed as a result of Fe dissolution can diffuse slowly and distribute evenly around the steel-concrete interface. As a result, the corrosion layer area was found to be the maximum for WDP. After a sufficient build up of expansive stress, the cover cracks.

### 3.4 Distribution of corrosion products along the steel-concrete interface

Figs. 5-7 show the heterogeneous distribution of corrosion products around the steel-concrete interface. The corrosion was only confined to concrete cover side where the chloride source was present. A generic corrosion structure to represent the samples would be: steel substrate- corrosion layer – corrosion affected paste – cement paste (S-CL- CP- P). This is in accordance with previous studies(Wong et al., 2010) that corrosion products are initially stored within the pores of cement paste (causing leaching of portlandite) and air voids followed by an accumulation at the steel-concrete interface. Consequently, the radial pressure at the interface increases and concrete cover subsequently cracks.

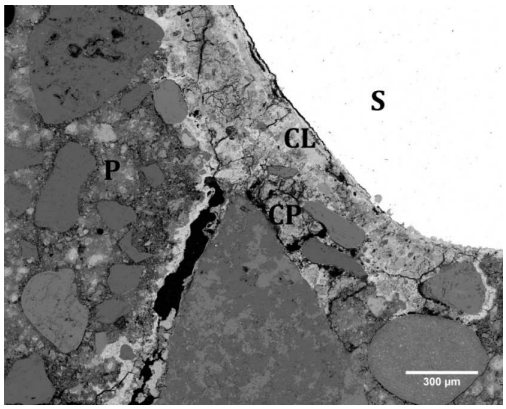


**Fig.5**: Typical corrosion structure i.e. **steel substrate- corrosion layer – corrosion affected paste – cement paste** for all samples.

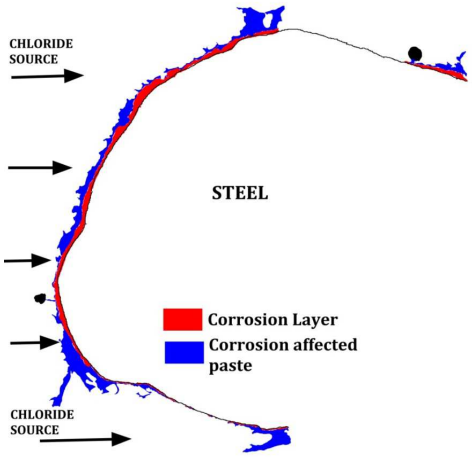


**Fig.6a**: Distribution of corrosion products for 1R.

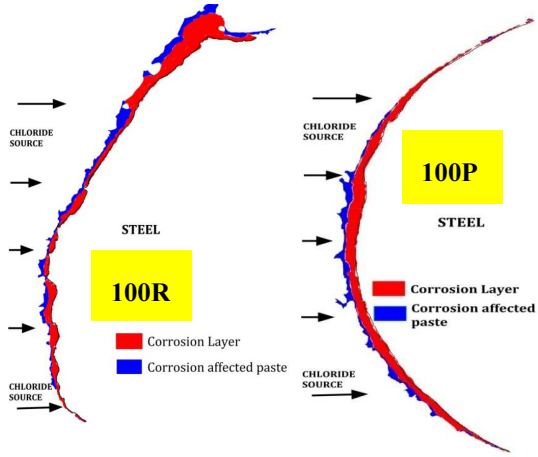


**Fig.6b**: Distribution of corrosion products for 100R and 100P.

Fig 5 shows that the corrosion product penetrated the aggregate-paste interface i.e. ITZ which is a structurally inferior region of the paste containing a large porosity. However, the rust products failed to penetrate the aggregates and provided an obstruction to the dissipation of iron oxides into the paste.

The formation of CL is influenced heavily by the presence of micro-cracks and porosity in paste which provide the necessary oxidation required by the intermediary chloro-complexes i.e. green rust (Sagoe-Crentsil&Glasser, 1993). From Fig 6, it can be seen that at certain regions the thickness of CL is more as compared to other. It is possible that these represent the regions of variable porosity where the pitting corrosion may have initiated due to an increased ingress of chloride ions, oxygen and moisture eventually leading to a generalized corrosion usually seen on rebars (Broomfield, 2007). It was also interesting to note that corrosion structure suggested previously (S-CL-CP-P) may not always be followed. There were instances where no penetration of rust products into the cement paste was observed despite accumulation of these products at the steel-concrete interface. This observation further justifies previous study by Wong et al., 2010 who found that corrosion products did not have any preferential location for their distribution along the steel-concrete interface.

**Comparison of 100R and 100P**: The 100P sample seems to have an even spread of CL as compared to 100R (Fig. 6b) which is possibly due to the presence of bearings on ribbed bar surface which may hinder the uniform corrosion product distribution.

**Comparison for impressed current and WDP samples:** The corrosion structure proposed before is applicable to WDP sample as well (Fig. 7) which indicates that **accelerated corrosion tests provide a good simulation of the natural conditions** to study the corrosion process of steel in concrete. However, the extent of CL obtained in alternate wetting/drying is found to be very high compared to impressed current tests. The lower corrosion rates seen in real size structures cause a gradual dissipation of $Fe^{2+}$ and $OH^-$ across the steel-concrete interface allowing gradual build up of stresses. This is analogous to slower load application which would cause the structure to creep and deform more. Similarly, an increased strain at the steel-concrete interface due to the lower corrosion current would result in a greater storage of corrosion products and hence, a thicker, homogeneously spread corrosion layer would be produced.

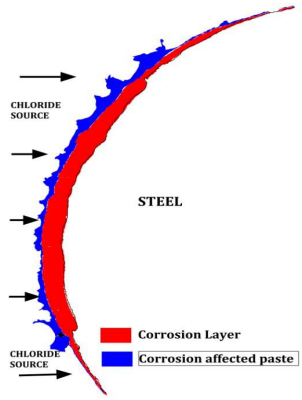


**Fig.7**: Distribution of corrosion products for WDP.

### 3.5 Quantitative EDX microanalysis for corrosion layer for samples 1R, 10R, 100R

Fe/O ratio for 100R is found to be lower than 10R which indicates that the outer CL region for 100R is more oxidised as compared to 10R (Table 7). This is consistent with the previous conclusion that higher oxidation levels for 100R sample (possibly caused due to higher micro-cracking) may have resulted in the formation of higher volume iron oxides causing cover cracking. On the other hand,

10R seems to have a reduced level of oxidation suggesting the formation of lower volume iron oxides on its interface (as compared to 100R); implying that it would need a greater accumulation of such corrosion products in order to develop necessary stress needed to cause crack initiation.

**Table 7:** Quantitative EDX microanalysis for outer CL region for impressed current (ribbed) samples

| **Sample** | **Mean atomic Fe/O ratio** |
|---|---|
| 1R | 0.91 ± 0.05 |
| 10R | 0.89 ± 0.07 |
| 100R | 0.68 ± 0.07 |

## 4 Discussion

### 4.1 Appraisal of impressed current samples having ribbed bar

It was seen that the 100R sample had the highest micro-cracking which is indicative of the faster build up of stress caused due to perhaps a faster diffusion of chloride ions into the cement paste. This micro-cracking plays a role in relieving the stress partially which causes surface crack width to reduce. Thus, this provides a possible explanation so as to why the average surface crack width was lower at 100 $\mu A/cm^2$ compared to 10 $\mu A/cm^2$.

Another notable finding was the comparable steel loss obtained for 10R and 100R sample. Faraday's law suggests that the amount of steel loss/degree of corrosion should increase significantly (around 200%) once the corrosion current density increases from 10 to 100$\mu A/cm^2$. However, this was not the case. 10R and 100R sample had quite similar steel section loss, degree of corrosion, CL% and CP% which made them very comparable. the cover cracking of 100R could be attributed to the accumulation of fewer high-volume corrosion products whereas 10R sample formed higher amount low-volume corrosion products. A higher amount of low-volume corrosion products would mean higher dissolution of iron as observed in the case of 10R. Thus, the application of Faraday's law especially at higher corrosion rates need to be reviewed where other factors such as the micro-cracking may have an influence on the amount of steel section lost. There is another opinion which says that the density (thickness) of corrosion products at higher corrosion rates may affect the rate of rust growth (El Maaddawy&Soudki, 2003; Liu &Weyers, 1998) which further questions the applicability of Faraday's law at higher current densities. Other studies have raised concerns regarding the accuracy of Faraday's law to predict steel loss at low chloride concentration and high impressed current due to the competing reaction taking place at anode (Nossoni&Harichandran, 2012).

The corrosion distribution figures showed that the corrosion products do not have any preferential location and can migrate anywhere into pastes, voids, micro-cracks which in turn depend on the diffusion potential of $Cl^-$, oxygen and moisture.

### 4.2 Corrosion pattern for ribbed and plain bar specimens

For similar corrosion current, the ribbed bar showed higher degree of corrosion as compared to the plain bar specimens which is consistent with previous findings possibly due to the presence of gaps under the ribs in deformed bars(Mohammed et al., 2001).

The uniform distribution of corrosion products along the rebar diameter can be ascribed to the absence of imperfections and bearings on the plain bars which may hinder the diffusion of $Fe^{2+}$/ $OH^-$ into the paste.

### 4.3 Appraisal of impressed current technique versus alternate wetting/drying

Impressed current techniques have been used before to accelerate the corrosion process and reduce the

time for crack initiation. Although it has a different electrochemistry behind its mechanism as compared to natural wet/dry process, it provides a good control to de-passivate steel within a few days (Austin, Lyons &Ing, 2004). It was observed that the corrosion structure, Steel-Corrosion Layer-Corrosion affected paste – Unaffected paste, was similar to the one obtained under natural conditions. The heterogeneous distribution of corrosion product for impressed current sample also matched very well with the WDP sample. However, the degree of corrosion was found to be very high in WDP case as compared to any of the impressed current samples. This was expected as the prolonged period of testing in case of WDP ensured that the sample was highly oxidized leading to the formation of higher volume iron oxides.

It was also manifested that the micro-cracks generated as a result of expansive stress acted as storage sites for corrosion products in case of WDP sample which was not quite visible in the case of impressed current specimens owing to their reduced corrosion times. Nevertheless, the corrosion products were found to penetrate the ITZ in the impressed current samples which is a highly porous region within the cement paste. Despite concerns over the tendency of impressed current technique to raise the electrochemical potential beyond the natural values causing an artificial polarisation of steel and reduced sensitivity to thermodynamic changes (Austin, Lyons &Ing, 2004), it offers the best alternative to simulate natural corrosion process in laboratory as it saves time and money.

### 4.4 Scope for future work

Although impressed current technique offered a good simulation to natural conditions, the elemental composition (like Ca, Fe, Si, O, Mg, Al) within CL and CP may be different owing to the different electrochemistry and corrosion times. Thus, there is a need to carry out a detailed SEM/EDX micro-analysis on the impressed current and alternate wet/dry samples in order to better appreciate the micro-chemistry involved.

Impressed current cathodic protection is one of the most popular electrochemical repair methods to inhibit corrosion. Using this method in laboratory by simply reversing the polarities, would provide a better understanding of the corrosion product distribution by using such a treatment. A possible approach could be to interchange the anode and cathode once the crack initiates so that the steel acts as a cathode and compare it with another specimen where the corrosion test is allowed to continue beyond the crack initiation stage. This would further enhance the current understanding regarding the micro-chemistry and elemental distribution in the microstructure when cathodic protection is used in real size structures.

## 5 Conclusions

Within the realms of the current study, the following wider conclusions can be drawn:

a) The degree of corrosion did not increase proportionately with an increase in impressed current as suggested by the Faraday's law. This suggests that Faraday's law linking corrosion current with steel section loss must be used with caution especially at higher current densities. Other micro-structural factors such as micro-cracking, denser accumulation of corrosion product (affecting the migration of $Fe^{2+}$ /$Fe^{3+}$/ $OH^-$) may have a significant influence on the steel loss at higher corrosion rates.

b) The plain rebar specimen was found to have a lower degree of corrosion than the ribbed bar specimen possibly due to presence of bearings/imperfections on the surface of the ribbed bar which affects the dissipation and migration

potential of the corroding species. Consequently, the corrosion products were evenly distributed close to the concrete cover for the plain bar specimen as compared to ribbed bar.

c) It was seen that impressed current technique offered a good alternative to alternate wet/dry process as the corrosion distribution structure and method of attack was similar in both cases. Green rust which converted into reddish-brown corrosion products was observed for both samples. However, very scant diffusion of corrosion products into the micro-cracks was seen in the case of impressed current specimen. Although, there have been concerns over the tendency of impressed current to cause artificial polarisation of steel, it still offers faster and economic means of simulating real size structural corrosion.

d) Further research needs to be conducted on studying the elemental distributions for the impressed current and wet/dry specimens which would offer us enhanced insight into the microchemistry, porosity involved and provide further validation of the impressed current technique to be used in service life model development.

**Acknowledgements**

The lead author would like to express his deepest appreciation towards **Dr. H. S. Wong** for his supervision, advice and magnanimity. The lead author owes his most sincere gratitude to **Mr. Young Han Shin**, his secondary guide, for helping him prepare the samples and easing him into the research. His generosity of spirit and unflinching encouragement enabled the author to finish this project with conviction.

**References**

Allan, M. L. (1995) Probability of corrosion induced cracking in reinforced concrete. *Cement and Concrete Research.*25 (6), 1179-1190.

Andrade, C., Alonso, C. & Molina, F. J. (1993) Cover cracking as a function of bar corrosion: Part I - Experimental test. *MateriauxEt Constructions.* 26 (162), 453-464.

Austin, S. A., Lyons, R. &Ing, M. J. (2004) Electrochemical behavior of steel-reinforced concrete during accelerated corrosion testing. *Corrosion.*60 (2), 203-212.

Bazant, Z. P. (1979) Physical model for steel corrosion in sea structures applications. *Journal Structural Division, ASCE.* 105 (6), 1155.

Bentur, A., Diamond, S. &Berke, N. S. (1997) *Steel corrosion in concrete.Fundamentals and Civil Engineering Practice.*1st edition. London, E & FN Spon.

Broomfield, J. P. (2007) *Corrosion of steel in concrete, understanding, investigation and repair.* second edition. London, Taylor and Francis.

Cabrera, J. G. (1996) Deterioration of concrete due to reinforcement steel corrosion. *Cement and Concrete Composites.*18 (1), 47-59.

Care, S. &Raharinaivo, A. (2007) Influence of impressed current on the initiation of damage in reinforced mortar due to corrosion of embedded steel.*Cement and Concrete Research.*37 (12), 1598-612.

Chen, D. &Mahadevan, S. (2008) Chloride-induced reinforcement corrosion and concrete cracking simulation.*Cement and Concrete Composites.*30 (3), 227-38.

El Maaddawy, T. A. &Soudki, K. A. (2003) Effectiveness of impressed current technique to simulate corrosion of steel reinforcement in concrete.*Journal of Materials in Civil Engineering.*15 (1), 41-47.

Goldstein, J., Newbury, D. E., Joy, D. C. & et, a. (2003) *Scanning electron microscopy and X-ray microanalysis.* 3rd edition. New York, Kluwer Academic/Plenum Publisher.

Gonzalez, J. A., Andrade, C., Alonso, C. &Feliu, S. (1995) Comparison of rates of general corrosion and maximum pitting penetration on concrete embedded steel reinforcement. *Cement and Concrete Research.*25 (2), 257-264.

Jaffer, S. J. & Hansson, C. M. (2009) Chloride-induced corrosion products of steel in cracked-concrete subjected to different loading conditions. *Cement and Concrete Research.*39 (2), 116-125.

Jensen, O. M., Hansen, P. F., Coats, A. M. &Glasser, F. P. (1999) Chloride ingress in cement paste and mortar. *Cement and Concrete Research.*29 (9), 1497-1504.

Liu, Y. P. &Weyers, R. E. (1998) Modelling the time to corrosion cracking in chloride contaminated reinforced concrete structures. *ACI Materials Journal.*95, 675.

Mangat, P. S. &Elgarf, M. S. (1999) Flexural strength of concrete beams with corroding reinforcement. *ACI Structural Journal.*96 (1), 149-158.

Mohammed, T. U., Otsuki, N., Hisada, M. & Shibata, T. (2001) Effect of crack width and bar types on corrosion of steel in concrete.*Journal of Materials in Civil Engineering.*13 (3), 194-201.

Nossoni, G. &Harichandran, R. S. (2012) Current Efficiency in Accelerated Corrosion Testing of Concrete.*Corrosion.*, .

Poupard, O., L'Hostis, V., Catinaud, S. &Petre-Lazar, I. (2006) Corrosion damage diagnosis of a reinforced concrete beam after 40 years natural exposure in marine environment. *Cement and Concrete Research.*36 (3), 504-520.

Rasband, W. (1997) *ImageJ*(1.47a) [Image Analysis Software] Maryland (US), National Institutes of Health.

Sagoe-Crentsil, K. &Glasser, F. (1993) 'Green rust' iron solubility and the role of chloride in the corrosion of steel at high pH.*Cement and Concrete Research.*23 (4), 785-791.

Tuutti, K. (1982) *Corrosion of steel in concrete.* Stockholm, Sweden, Swedish Cement and Concrete Research Institute. Report number: 4.

Wong, H. S., Zobel, M., Buenfeld, N. R. & Zimmerman, R. W. (2009) Influence of the interfacial transition zone and microcracking on the diffusivity, permeability and sorptivity of cement-based materials after drying. *Magazine of Concrete Research.*61 (8), 571-589.

Wong, H. S., Zhao, Y. X., Karimi, A. R., Buenfeld, N. R. & Jin, W. L. (2010) On the penetration of corrosion products from reinforcing steel into concrete due to chloride-induced corrosion. *Corrosion Science.* 52 (7), 2469-2480

Zhao, H. & Darwin, D. (1992) Quantitative backscattered electron analysis of cement paste. *Cement and Concrete Research.*22 (4), 695-706.